7.7 HIGH RESOLUTION FUTURE SCENARIO CLIMATE DATA FOR NORTH AMERICA

David T. Price[1*], D. W. McKenney[2], P. Papadopol[2], T. Logan[l], M. F. Hutchinson[3]
[1] Canadian Forest Service, Edmonton, Alberta dprice@nrcan.gc.ca; tlogan@nrcan.gc.ca
[2] Canadian Forest Service, Sault Ste. Marie, Ontario dmckenne@nrcan.gc.ca; ppapadop@nrcan.gc.ca
[3] Centre for Resource and Environmental Studies, The Australian National University, Canberra, Australia

1 ABSTRACT

Eight monthly climate scenario data sets covering North America at ~10 km resolution were constructed using General Circulation Model (GCM) output from four models (Canadian CGCM2, UK HadCM3, Australian CSIRO Mk2 and European Union ECHAM4). Each data set included a projection for the period 1991-2100, forced by one of the IPCC SRES A2 and B2 emissions scenarios. GCM variables were monthly precipitation and solar radiation, mean vapour pressure and wind speed, and mean daily minimum and maximum temperatures. Data were first normalized to differences (temperature), or ratios (other variables), of the means for the simulated period 1961-90. These monthly "delta" terms were then interpolated as functions of latitude and longitude using thin-plate smoothing splines as implemented in ANUSPLIN. The resulting spline surfaces were used to create monthly grids at 0.08333º latitude/longitude resolution. These were combined with interpolated maps of observed 30-year climate normals, to produce physically consistent gridded scenarios of future climate. Each combines spatial variability observed in present-day climate with the spatio-temporal variability simulated by one GCM. Averaged across North America, results (reported here for temperature and precipitation only) reveal quite consistent long-term trends, particularly in the GCMs' differential responses to the A2 and B2 emission scenarios. The scenarios differ more in their projections of interannual variability, both compared to historical data and in their responses to greenhouse gas forcing. Maps of selected data at 0.5º resolution reveal rich spatial structure dominated by elevation effects on observed climate, but vary in details due mainly to differences among the GCMs. The data sets will be useful for assessing impacts of transient changes in climate on ecosystems and other studies where long-term projections of future climate are required.

2 INTRODUCTION

The potential broad-scale (i.e., regional to global) impacts of climate change on natural ecosystems can only be investigated using spatially distributed ecosystem process models that respond realistically to climatic factors. While the development of suitable ecosystem models is an active area of research, at some stage it is necessary to drive these models with plausible forecasts of future climate. This objective can be addressed in several ways, depending on the questions being posed and the type of model being used (e.g., see discussion by Bugmann et al., 2000), though for many purposes, the most plausible forecasts of future climate originate from simulations carried out using general circulation models (GCM).

Several approaches to creating scenarios of future climate from GCM data are in use. These include statistical and dynamical downscaling and the use of Regional Climate Models (RCM), as well as statistical interpolation. RCMs are fully dynamical models driven by lateral boundary conditions imposed by a "host" GCM (e.g., Laprise et al. 2003). Other downscaling methods attempt to correlate large-scale atmospheric processes to local scale meteorology and apply this information to GCM projections of future weather patterns to characterize future local scale climate, e.g., Statistical DownScaling Model (SDSM) of Wilby et al. (1998, 2002). Such approaches attempt to maintain physical consistency with the GCM representations of atmospheric processes, and can generate high frequency simulated meteorological data suitable for many applications (e.g., to drive agricultural crop models). At present, however, they are generally too computationally expensive for routine production of multiple scenarios covering large regions over periods of several decades or centuries.

Statistical interpolation of GCM output is a simpler approach to obtaining estimates of climate variables at locations between climate stations. Although lacking the physical detail of dynamical downscaling or RCMs, these methods develop physically-based statistical relationships that can be applied over large regions to provide scenario data sets that both capture the climate change signals simulated by the GCM, and remain spatially and temporally consistent among variables (see also discussion in Houser et al., 2004). Moreover, the GCM data can be normalized to remove bias and hence make the scenarios broadly consistent with observations.

Nalder and Wein (1999) reviewed several conventional methods of interpolating climate observations, while Price et al. (2000) performed a rigorous comparison of Nalder's GIDS method with the thin plate smoothing spline routines (ANUSPLIN) of Hutchinson (2000) applied to extensive regions within Canada. These studies demonstrated that mean monthly climate data can be interpolated quite accurately where climate station observations are lacking, and that the expected error in the interpolated estimate can be quantified.

[*] *Corresponding author address*: David T Price, Canadian Forest Service, Edmonton, Alberta.
e-mail: dprice@nrcan.gc.ca

One attraction of statistical interpolation for downscaling GCM scenario data is that it allows rapid construction of data sets suitable for driving ecological models at spatial resolutions comparable to major landscape features, soil polygons and small catchment basins. These data sets are comparable to those available from RCM simulations (50 km or less), but they can be created using GCM data available freely from sources such as the Intergovernmental Panel on Climate Change (IPCC) Data Distribution Centre (DDC) [see http://ipcc-ddc.cru.uea.ac.uk/dkrz/dkrz_index.html].

Downscaled GCM data have been used in large-scale simulations of responses of vegetation to future climate in the USA and Canada, but to our knowledge, no studies covering all of North America have yet been reported. Furthermore, many of the regional simulations, particularly those carried out in Canada, have not used the same climate data, even where GCM or regional climate model (RCM) output were available, thus making it difficult to compare the results of these studies. To date, most national-scale studies for Canada (e.g., Rizzo and Wiken 1992; Lenihan and Neilson 1995) have been based on equilibrium projection simulations (i.e., static vegetation responding to a stable climate). Such studies cannot capture the transient effects of ecological processes that will likely respond to variations and long-term trends in climate. More recently, the Intergovernmental Panel on Climate Change supported simulations for Canada based on transient climate projections obtained from fully-coupled GCMs (Neilson, 1998). The VEMAP project (VEMAP members, 1995) similarly compared national scale impacts of climate change on vegetation attributes in the USA using a suite of different climate scenarios derived from GCM simulations (see also Kittel et al. 1997).

Here we report the development of a consistent set of climate scenarios, derived from four different GCMS, and two IPCC SRES emissions scenarios, covering the entire area of continental North America at ~10 km grid resolution. These scenarios are based on statistical interpolation of present-day climate observations, including elevation effects, combined with interpolation of GCM simulation data to capture the “climate change signal” due to increases in atmospheric greenhouse gases (GHG). Each of these eight scenarios provides, for the given projection of GHG and aerosol emissions, a consistent climate data set on a monthly time interval, extending for the period 1961-2100—although where data were available for the period prior to 1961, these are also provided. The scenario data themselves are interpolated differences (in the case of temperature) or ratios (in the cases of radiation, precipitation, wind and vapour pressure) referenced to the respective simulated means for the 1961-90 period. These data were treated as anomalies for each variable and combined with grids of interpolated monthly mean data for North America for the same 1961-90 period. The scenarios so generated thus provide a set of spatially detailed, and internally consistent, projections of changes in North American climate relative to 1961-90, as captured by several state-of-the-art GCMs.

3 DATA AND METHODS

3.1 Baseline climate data

Climate records for several thousand stations across North America were combined into single data sets for a variety of analyses. These included 1961-90 monthly mean daily maximum and minimum temperature (T_{max} and T_{min}, respectively), precipitation, windspeed and relative humidity. Monthly mean surface-incident solar radiation data were combined for 56 Meteorological Service of Canada stations and data available for 55 stations from the US National Energy Research Laboratory. For each variable, ANUSPLIN was used to generate regular grid spatial models. Most of these involved treating station latitude, longitude and elevation as independent variables. For example, solar radiation was developed as a rainfall-dependent surface with, rainfall acting as a surrogate for cloudiness (see Hutchinson, 2000). Although vapour pressure (*e*) was the preferred humidity variable, these data were not available from the US National Climate Data Centre. Instead, monthly mean relative humidity data were interpolated to the 0.0833º latitude/longitude grid, and later converted to estimates of vapour pressure. Details on these models will be reported elsewhere but many can be viewed interactively at http://www.glfc.cfs.nrcan.gc.ca/landscape/climate_models_e.html.

3.2 GCM data: downloads and pre-processing

Data were downloaded for four GCMs (Canadian Climate Centre for Modelling and Analysis (CCCma), CGCM2, UK Hadley Centre HadCM3; Australian CSIRO Mark 2 GCM; and Max Planck Institut für Meteorologie ECHAM4) for two IPCC SRES emissions scenarios (A2 and B2, see IPCC, 2000). In each case, the data sets included six monthly climate variables (maximum and minimum temperature, [T_{max} and T_{min}, respectively], precipitation, total downward solar flux at surface, wind velocity (2 m or 10 m height) and a humidity variable. In the case of the CGCM2, for which multiple “ensemble” runs had been performed with different initializations, only results for the *second* run were used.

A procedure was developed to standardize, as far as possible, the extraction of the GCM scenario data for each climate variable and to reorganize them into a format suitable for input to ANUSPLIN (see below). To develop the higher resolution spline models, each GCM grid node was treated as if it was a climate station, with each line of input data containing grid node longitude, latitude and elevation (the latter taken from the GCM orography file, but not used in the procedures reported here), followed by 12 monthly data values. A custom program, GCM_PROCESSOR2 (first reported in Price et al., 2001), was then used to remove GCM bias (relative to observations) in a two-pass procedure. On the first pass, 30-year means were calculated for each month during the simulated period. On the second pass, the mean simulated values for each month in 1961-1990 were then either subtracted from (T_{min} and T_{max}), or divided into (other variables), the modelled monthly data to generate the delta values (or simulated monthly anomalies) for the entire simulation period.

In the particular case of humidity data, the preferred measure was vapour pressure, which required conversion from other measures that differed among the GCMs: CGCM2 and CSIRO both report specific humidity; HadCM3 reports relative humidity and ECHAM4 dewpoint temperature. Because vapour pressure is elevation-dependent, it was necessary to download modelled sea-level pressure data to provide barometric corrections. A second custom program, ANU_HUM, was written to perform the conversion of humidity data for each GCM to vapour pressure units.

The details of the preprocessing procedures varied amongst the different GCMs, and are outlined in the following sections.

3.2.1 CCCma CGCM2

Input data were downloaded from the Canadian Centre for Climate Modelling and Analysis (CCCma) at http://www.cccma.bc.ec.gc.ca/data/cgcm2/cgcm2.shtml This website allows regional subsets to be extracted online. Each file was obtained in a 6-column floating point ASCII format, with each monthly time step separated by a header line. The subset domain grid was in geographic projection, with nominal cell dimensions of 3.75º longitude × 3.71º latitude, covering the region 168.75º to 52.50º W, 16.70º to 83.48º N (32 cells E-W by 19 cells N-S) covering North America and part of Greenland. CGCM2 runs for each IPCC SRES scenario consist of a common period 1900-1990 (as used for the IS92A “greenhouse gas (GHG) plus aerosol” integration), followed by separate simulations for 1991-2100. Data for 1990 were removed from each of the A2 and B2 datasets, and the GHG+A and A2 or B2 datasets then concatenated to create a single dataset for each of the A2 and B2 scenario simulations for 1900-2100.

Vapour pressure data were derived from specific humidity and sea-level pressure data downloaded from the CCCma website. The conversion algorithm consisted of the following steps:

1. Read in T_{min}, specific humidity (q, kg kg^{-1}) and sea-level pressure (hPa) for each GCM gridpoint.
2. Adjust sea-level pressure to “surface pressure” at the elevation given by the CGCM2 orography data, using equation from R.L. Snyder at http://biomet.ucdavis.edu/conversions/humidity_conversion.htm]

   $$P(z) = P(0)/[(1.0 - 0.0065z/293.0)^{5.26}] \quad [1]$$

   where $P(z)$ is the atmospheric pressure at elevation z (metre), and $P(0)$ is the pressure at sea-level obtained from the CGCM2 data archive.
3. Calculate vapour pressure, e, from specific humidity and surface pressure using:

   $$e = \mathrm{P}(z)\, q/[0.622(1.0 - q(1.0 - 1.0/0.622))] \quad [2]$$

   where 0.622 is the ratio of the molecular weights of water vapour to air.
4. Calculate saturation vapour pressure e^* (kPa) at T_{min} using polynomial equations of Lowe (1977).
5. Ensure that vapour pressure does not exceed e^* at T_{min}, as determined by CGCM2 for the grid cell. This requires that the value of e^* also be adjusted to the elevation obtained from the CGCM2 orography data. I.e.,

   $$e(z) = \min\{\, e,\ e^*(T_{min})\ P(z)/P(0)\,\} \quad [3]$$

The resulting vapour pressure data were then normalized and interpolated as for all other GCM variables.

3.2.2 UK Hadley Centre HadCM3

Data were downloaded in GRIB format from the IPCC DDCData Distribution Centre web site, with topography and grid information and the GRBCONV program source code (for Sun Solaris 2.5) [found at http://www/dkrz.de/ipcc/ddc/html/HadleyCM3/hadcm3.html] The GRBCONV program was used to convert the data files from GRIB format to the more conventional 6-column floating point ASCII. The download site does not offer the option to subset the data based on an area of interest, so a custom program GCM_SUBSET was used to extract the data for the region of interest. The HadCM3 topography data were used to construct files containing longitude, latitude and elevation information, with cell dimensions 3.75° longitude and 2.5° latitude, covering the region from 168.75º to 52.50º W, 15.00º to 85.00º N (32 cells E-W by 29 cells N-S).

The Hadley Centre performed separate integrations with the HadCM3 for each of the IPCC SRES A2 and B2 scenarios for the entire period 1950-2099. Hence, the data HadCM3 interpolated for 1950-1990 also differed between the two scenarios—which had an important implication when comparing the results.

In the particular case of the wind speed field for the HadCM3 model, the grid nodes are located midway between the latitudinal coordinates of the grid nodes used for the other variables, so a separate set of coordinates was built: from 168.75º to 52.50º W, and from 13.75º to 86.25º N (32 cells E-W by 30 cells N-S).

Vapour pressure data were estimated from the HadCM3 relative humidity field using the following algorithm:

1. Read in T_{min} and T_{max}, and calculate the mean of these values (T_{mean}).
2. Read in relative humidity (RH) data (percent).
3. Calculate saturation vapour pressure e^* (kPa) at T_{mean} using Lowe (1977).
4. Calculate monthly mean vapour pressure, e, from

   $$e = e^*(T_{mean})(0.01RH) \quad [4]$$

5. Ensure that vapour pressure does not exceed e^* at T_{min}, as determined by HadCM3 for the grid cell, using Eq. 3.

3.2.3 CSIRO Mk2 GCM

Detailed description of the Australian CSIRO Atmospheric Research Laboratory GCM is available at http://www.dar.csiro.au/publications/hennessy_1998a.html#ccm). Data were downloaded from the IPCC DDC web site for five variables (T_{max}, T_{min}, in Kelvin, precipitation, incident solar radiation and windspeed). Surface specific humidity data were not available from the DDC but were instead requested directly from CSIRO in Melbourne (Tony Hirst, CSIRO Atmospheric Research, 2003, pers. comm.), together with sea-level pressure and T_{min} data. As a check, the T_{min} data downloaded from DDC was compared to those received directly from CSIRO and found to be identical.

As with HadCM3, subsetting was not possible online. All data were received in GRIB format for the years 1961-2100. GRBCONV was then used to convert these to 6-column ASCII and GCM_SUBSET was used to extract data for the North American region. Coordinate data were extracted from the CSIRO Mk 2 topography information: cells have nominal dimensions of 5.6° longitude by 3.2° latitude so the domain extended from 168.75° to 50.625° W and from 14.3357° to 87.5613° N (24 cells E-W by 21 cells N-S).

As with CGCM2 and HadCM3, the time-series data were split into two periods with the first 30 years (1961-1990) common to the integrations for both the IPCC A2 and B2 emissions scenarios.

Surface specific humidity were used to calculate vapour pressures at the grid cell elevation, exactly as was done for CGCM2 (eqs. 1-3).

3.2.4 Max Planck Institute (MPI) ECHAM4

As with HadCM3 and CSIRO Mk 2, data were downloaded in GRIB format from the IPCC DDC web site. ECHAM4 grid cells have dimensions of constant width but vary in the latitudinal dimension from 2.7906º at the Equator to 2.7673º at the poles. Hence, the North American subset area extended from 168.75º to 50.62º W and from 15.35º to 85.09º N (43 cells E-W by 26 cells N-S).

Monthly mean data were available for precipitation, surface-incident solar radiation, windspeed, dewpoint temperature and mean sea level pressure for the A2 and B2 emissions scenarios for 1991-2100, together with topography and grid information. A GRIB format processing program was also obtained from http://cera-www.dkrz.de/IPCC_DDC/SRES/ECHAM4/echam4opyc3.html.

Screen temperature data (T_{min} and T_{max}) were not available from IPCC-DDC, however, with a note on the website stating that prior to 23/10/2002 these data were erroneous. A request was made to CERA (Max-Planck Institute), and granted, for access to their on-line database at http://cera-www.dkrz.de/CERA/index.html to acquire the most recent T_{min} and T_{max} data.

Following advice from H. Luthardt (MPI, 2003, pers. comm.), the ECHAM4/OPYC3 GHG + sulphate aerosol experiment from MPI (MP01GS02 simulation) was selected as the integration for the period 1900-1990, for which data were also downloaded from IPCC-DDC and from CERA. These were inserted into each of the A2 and B2 integrations to make complete time series for the period 1990-2100. GCM_SUBSET was then applied to each data set, followed by GCM_PROCESSOR2 to convert the data to differentials from the means of the simulated 1961-1990 period.

Vapour pressure data were calculated from the dewpoint temperature data using ANU_HUM. In this case, the algorithm consisted of the following steps:

1. Read in screen-height T_{min} (K), and dewpoint temperature (T_{dew}, K) data.
2. Read in sea-level pressure data (in Pa), and adjust to surface pressure at the elevation given by the ECHAM4 orography, using eq. 1.
3. Calculate saturation vapour pressure, e * (kPa) at T_{dew}, taking this as the monthly mean vapour pressure.
4. Ensure that vapour pressure does not exceed e* at T_{min}, as determined by ECHAM4 GCM for the gridpoint, i.e.,

   $$e(0) = \min\{ e^*(T_{dew}), e^*(T_{min}) \} \quad [5]$$

   where $e(0)$ indicates vapour pressure at sea level. In this particular case, because e* will remain proportional to barometric pressure, it is not strictly necessary to correct for elevation here. Furthermore, it is really only necessary to ensure that $T_{dew} = T_{min}$ at all times.
5. Finally, adjust the value of $e(0)$ calculated at step 4 to the elevation of the grid point obtained from the ECHAM4 orography data in step 2:

   $$e(z) = e(0)\ P(z)/P(0) \quad [6]$$

3.3 *Interpolation using ANUSPLIN*

ANUSPLIN is a package of programs (Hutchinson, 2000) used to fit thin plate splines to noisy data, of which climate station records are a classic example. It has been applied successfully in Australia, New Zealand, China and parts of southeast Asia, South America, Africa, and Europe (e.g., Hutchinson, 1995, 1998a, 1998b), to Canada (Price et al. 2000; McKenney et al., 2001, 2004 this conference) and globally (New et al., 2002), to interpolate monthly means of several key climate variables, as well as to interpolate daily data (e.g., Hutchinson, 1999a). The general approach is to treat climate data as variables dependent upon spatial dimensions (latitude, longitude and elevation) and potentially other factors such as slope, aspect, and spatially varying rainfall distributions). Rigorous tests by Price et al. (2000) and McKenney et al. (2001) indicated that ANUSPLIN can perform extremely well for several key long-term mean climate variables across much of Canada. There remain challenges at shorter timesteps in remote areas at high latitudes and high elevations where climate stations are sparse and/or records are incomplete or of poor quality).

Thin plate splines can be described as a generalization of a multivariate linear regression model in which the parametric model is replaced by a smooth nonparametric function. The theory of ANUSPLIN has been described extensively elsewhere (e.g., Hutchinson, 2000, 1995, 1998a, 1998b; Hutchinson and Gessler, 1994), as well as briefly in McKenney et al. (2004, this conference), hence will not be discussed further.

In previous work (Price et al., 2001), several experiments were carried out to investigate different ANUSPLIN models and settings, relating particularly to the use of elevation as a third independent variable for statistical downscaling of GCM output. Statistics generated by ANUSPLIN in these tests showed that elevation had little effect on the fitted surfaces; i.e., there was no statistical signal in the interpolated anomaly values when elevation was included as the third independent variable. A possible explanation is that elevation is typically averaged across an entire GCM grid cell, so mountainous regions are reduced to relatively low altitude plateaux, and hence, the effects of dramatic changes in elevation (e.g., on temperature, rainfall and windspeed) are not captured well. It was therefore decided that the interpolation of GCM data would be based solely on longitudinal and latitudinal gradients, while any effects of elevation on local climate would be captured in the analysis of actual climate station records. In the latter case, elevation effects are clearly significant (e.g., McKenney et al. 2001). The bivariate ANUSPLIN interpolations reported here all used a constant smoothing parameter (fixed signal). Essentially individual GCM grid cell values are smoothed by this procedure, thereby including the influences of adjacent grid cells, and hence reducing the occurrence of singularities ("bullseyes"). This seems reasonable because the GCM outputs are inherently uncertain, and nearby grid cells are somewhat indicative of the likely changes that would drive landscape-scale changes.

Hence, ANUSPLIN was used to fit surfaces to the normalized monthly GCM scenario data treating them as if they were anomalies from the 1961-90 mean values. The companion program LAPGRD was then used for creating regular grids together with log files containing summary statistics. Each output grid contained interpolated anomalies for a land surface mask derived directly from a 300 arc-second digital elevation model (DEM) of North America constructed at the CFS Great Lakes Forestry Centre from Canadian 1:250,000 National Topographic Data (http://www.glfc.cfs.nrcan.gc.ca/landscape/topographic_models_e.html) using ANUDEM software (Hutchinson, 1989; see also http://cres.anu.edu.au/outputs/anudem.php), combined with the USGS GTOPO30 DEM coverage for the USA (http://edcdaac.usgs.gov/gtopo30/README.asp). The monthly climate grids were generated in ARC/INFO ASCII format, with a cell size of 0.0833º latitude × longitude, covering the domain from 168º to 52º W and from 25º to 85º N (1,392 columns × 720 rows).

3.4 Scenario data handling

The climate grids created by the interpolation of the monthly data were concatenated into time-series files. This required some programming effort, not least because the total size of each monthly time series at 0.0833º resolution is huge. For example, in the cases of the CGCM2 and ECHAM4 scenarios, there are 201 years of monthly data for each variable, giving a total of 2,412 monthly models (maps). Each monthly map contains over 1,000,000 grid cells. Hence, when multiplied by 2,412 months, the complete data set for a single variable contains about 2.5 billion data values (including the NO_DATA values for ocean pixels). Storing this in an ASCII format (4 significant digits plus separator) would require approximately 12.5 GB per variable. The total storage required for eight scenarios and six variables at this resolution would be about 500 GB.

One solution to this data-handling problem is to compress the data into a binary format. In past work, we adopted the University Corporation for Atmospheric Research (UCAR) network Common Data Form (NetCDF) standard to develop a series of UNIX tools for processing, storing and manipulating gridded data sets (http://www.unidata.ucar.edu/packages/netcdf/) see also Price et al., 2001). The NetCDF files are configured to store all values internally as 16 bit integers, allowing all 0.0833º resolution data for a single variable to be stored in a file of about 5 Gbyte per variable. This will work satisfactorily on any Unix system that can handle files greater than 2 GB, but still presents a problem on many systems at the present time. NetCDF data files can also be compressed to allow convenient storage and transmission via Internet. The NetCDF standard allows scaling and offsetting values to be applied to the internal data, to minimize any loss of precision.

For the present study, however, the high resolution data were aggregated up to 0.5º resolution using an ARC/INFO GRID macro. For each month, all 0.0833º data values falling within a 0.5º boundary were averaged (excluding NO_DATA values). These data were then converted to NetCDF format using a custom conversion program ASG2NC. Results presented here are all based on the 0.5º aggregated data.

To provide some reasonably clear pictures of the interannual trends, the normalized data from each scenario for each variable were first combined with the gridded 1961-90 climate normals data using a custom program NC_MERGE, which operates directly on data stored in NetCDF format. I.e., gridded climate data were *added to* the simulated anomalies in the case of temperature, but *multiplied by* the simulated ratios obtained for other variables. Selected examples of these merged grids were then used to create GIF format maps of simulated future climate using another program NC2GIF. These data were also aggregated into spatial averages for the North American continent using a program called NC_AGGREGATE, and converted to time-series of seasonal averages using a program called NC_AVERAGE (where March-May is "spring"; June-August is "summer"; September-November is "fall" and December-February is "winter").

4 RESULTS

Here we present a few selected samples of the results obtained, limited to analyses of temperature and precipitation data. They are designed to illustrate the richness of the data, their spatial and temporal resolutions, and some of the trends and variability characteristics that have been captured from the different GCMs.

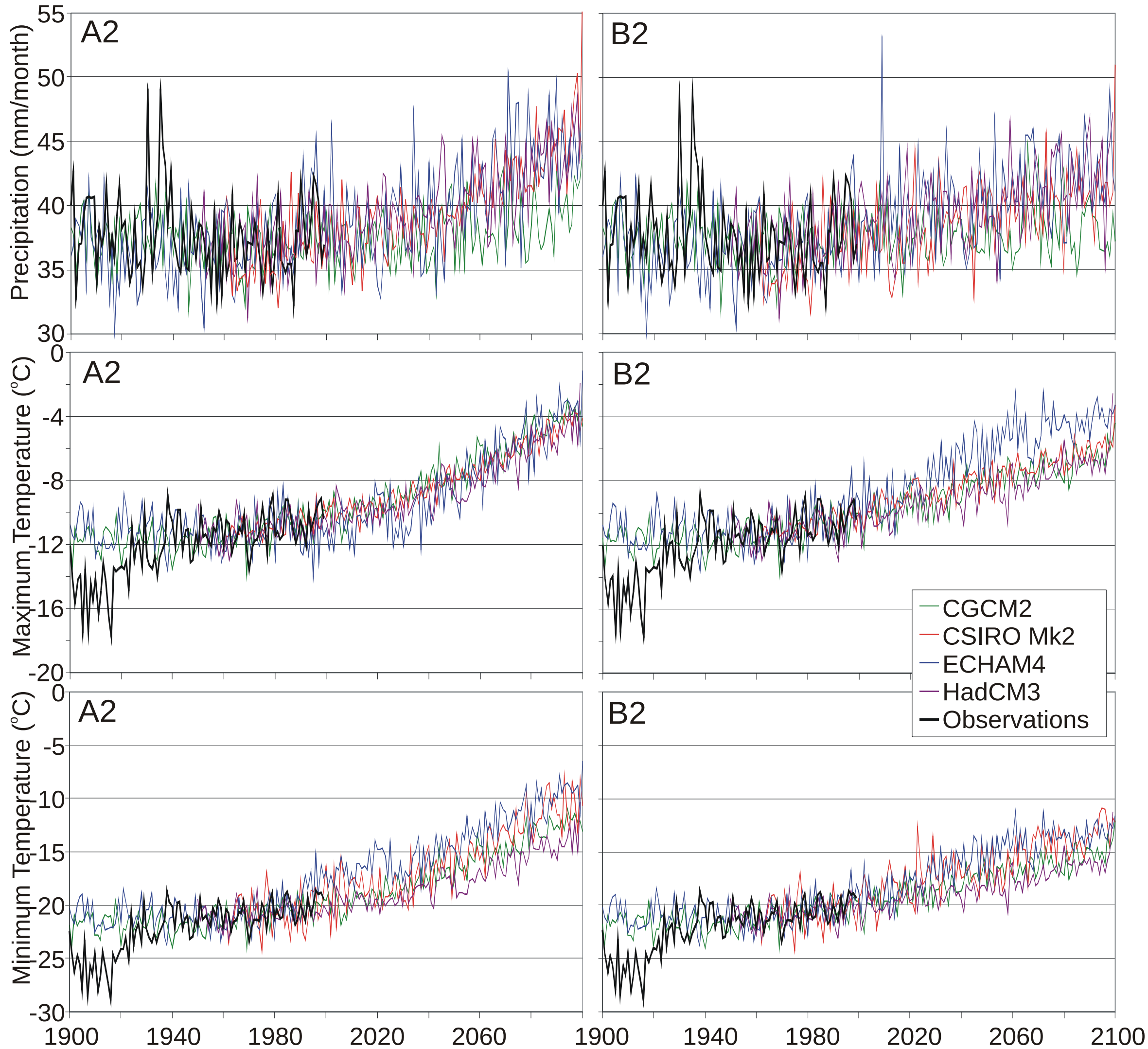

Figure 1. Comparison of GCM scenarios interpolated to 0.0833º resolution for winter season (December, January, February) aggregated for the land area of continental North America. All GCM simulations were forced with IPCC SRES emissions scenarios, (left A2, right B2). For comparison, historical data for the period 1901-2100 are also shown, similarly aggregated from 0.0833º interpolated data. All data are normalized to the observed 1961-90 means.

Figures 1-2 compare the simulated changes in winter and summer temperature and precipitation as forecasted by each GCM under each of the IPCC SRES A2 and B2 emissions scenarios. Also shown for comparison is a reconstruction of historical data. It should be remembered, however, that these graphs represent a spatial aggregation across the entire North American continental land area, so regional trends may differ appreciably from those shown here.

Some discrepancies in the historical data for the first half of the 20th century (summer maxima were evidently warmer, and winter minima, cooler, than after 1950) may be attributed to the spatial averaging of the data, which does not account for latitudinal differences in grid cell area (to be discussed later). It should be emphasized that the interpretation of the historical record was not an objective of this study, and is to be addressed in detail in another paper. The most important objective here was to assess the general trends and variability that can be seen in the historical records and compare these with the trends and variability seen in each GCM scenario.

With these important caveats in mind, the continent-wide trends seen in most of the scenarios derived from the GCM simulations correspond fairly well to the historical record, at least for the period after

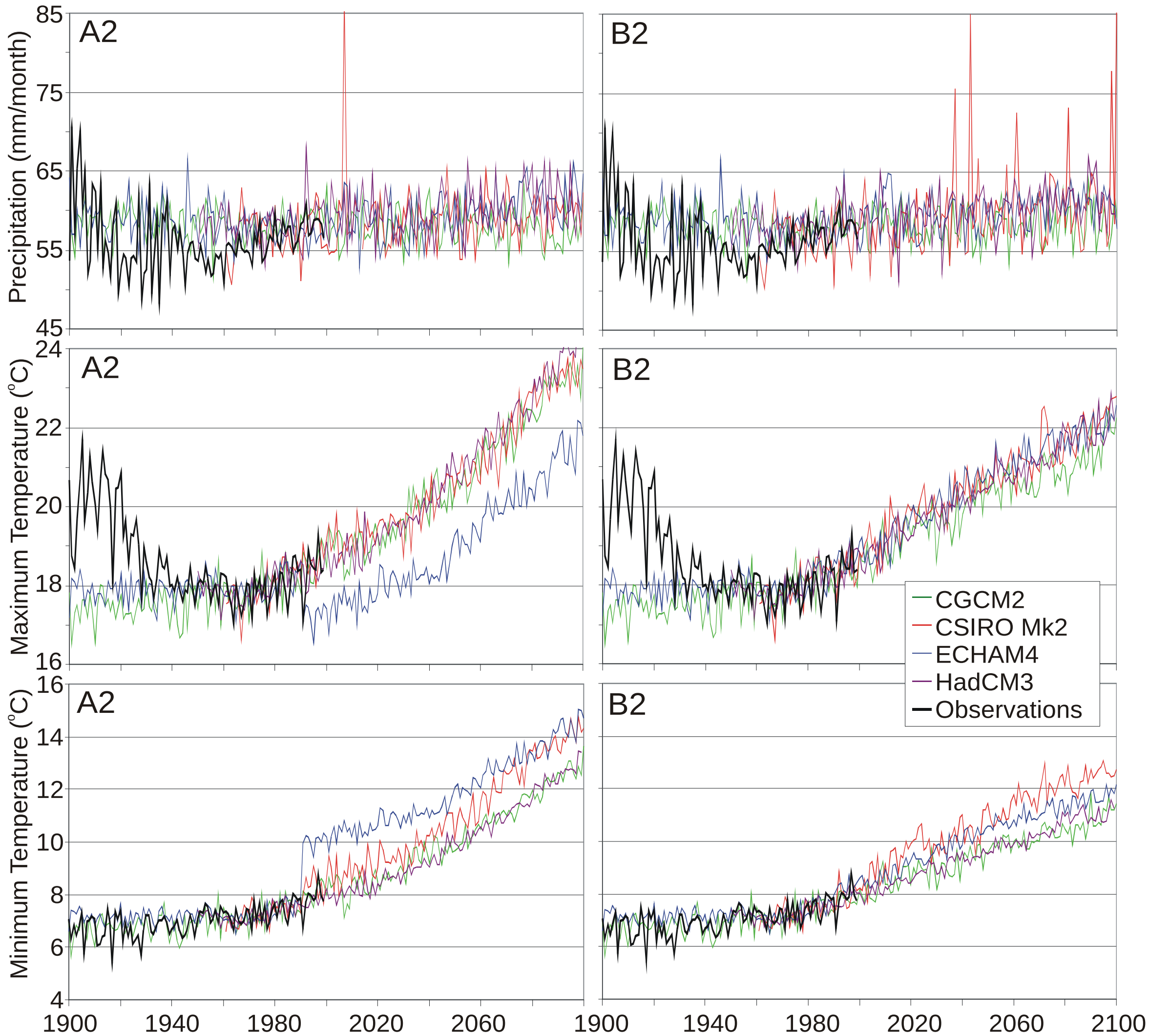

Figure 2. Comparison of GCM scenarios interpolated to 0.0833º resolution for summer season (June, July, August) aggregated for the land area of continental North America. All GCM simulations were forced with IPCC SRES emissions scenarios, (left A2, right B2). For comparison, historical data for the period 1901-2100 are also shown, similarly aggregated from 0.0833º interpolated data. All data are normalized to the observed 1961-90 means.

1950. There are two notable exceptions: First, the ECHAM4 A2 scenario produces marked steps in the summer temperature data (decrease in T_{max} and increase in T_{min}), that appear unrealistic. Second, the CSIRO Mk 2 GCM appears to project some extremely wet summers, where rainfall greatly exceeds any value reported in the historical record. This was traced to an interesting problem in the region close to the California coast, where the GCM simulates mean rainfall for some months close to zero for the 1961-1990 period (much lower than occurs in reality). It also projected significant increases (of the order of 10-20 mm month^{-1}) for the future, which resulted in absurdly high anomaly ratios for some months. When these ratios were multiplied by baseline observations, some enormous spikes in monthly rainfall were generated. Subsequently, 164 instances of ratios exceeding 10.0 were observed to occur in the B2 scenario simulation. The precipitation data obtained from the CSIRO Mk 2 should therefore be used cautiously. In future, a maximum threshold ratio will be imposed for variables such as this.

All the GCMs show marked increases in both summer and winter temperatures from 1991. As might be expected given the greater GHG forcing resulting from the A2 emissions scenario, the A2 simulations generally predict larger temperature increases. By

2100, the projected increases are approximately 6 ºC in summer and 8 ºC in winter for A2, compared to 4 ºC and 6 ºC for B2, respectively. (See also columns 6-9 in Table 1.) Furthermore, with the exception of ECHAM4 A2, the differences between emission scenarios are at least as significant as the differences among models. There also appears to be a consensus amongst the GCMs that winter precipitation will increase—by as much as 20% under the A2 scenario and 10% under the B2.

The assessment of changes in variability simulated by the different GCMs is difficult when based only on visual inspection of Figures 1 and 2. These graphs suggest that the GCMs generally produce lower inter-annual variability than observed, although the ECHAM4 appears to capture the year-to-year variations in temperature and precipitation quite well. The CGCM2 seems able to capture much of the interannual variability in precipitation but underestimates it for temperature.

Table 1 attempts to provide a more quantitative assessment of the GCM simulations of interannual climate variability. This table is divided into three sections, for each of minimum and maximum temperature and precipitation. In the first section (columns 2-5), variances of the means simulated by each GCM aggregated over the North American landmass, were calculated for each season in the 30-year period 1961-1990. Given that the observed historical mean values were also used as the baseline for normalizing all the GCM data, the means of all simulated and observed data for this period should be identical. (Furthermore, the variances obtained from the A2 and B2 emissions scenarios should be similar for each GCM because, the GHG forcings for the 1961-90 period are the same.) Table 1 therefore reports the *ratios* of the simulated variances to the observed variances. A value of 1.0 indicates near-perfect agreement between the modelled and observed variances. Values significantly less than 1.0 imply the model is underestimating variability, and conversely.

Table 1 shows that the variances obtained for the A2 and B2 scenarios for 1961-1990 were generally very similar although small differences can be detected. There are two contributing explanations: (1) in the particular case of the HadCM3, the integrations for the A2 and B2 scenarios were performed separately, so presumably some differences in initialization for these runs resulted in significant differences in the output for the 1950-1990 period; (2) winter values for all three variables often differ because they include data for January and February 1991 in the seasonal means.

It can be seen that the CSIRO Mk 2 greatly exaggerated variability in observed T_{min} for fall and winter, though perhaps surprisingly, it was quite accurate for spring and summer. The remaining GCMs significantly underestimated the variability in fall temperatures, but variability in winter spring and summer T_{min} were generally captured reasonably well. The success in capturing variability in T_{max} was more variable: most models underestimate, though CSIRO is reasonably good in summer and fall while ECHAM4 overestimates in winter and spring. CGCM2 and HadCM3 only achieved reasonable agreement in summer and spring, respectively.

For precipitation, Table 1 shows that with the exception of CSIRO Mk 2, all models generally underestimated variability in seasonal precipitation, although HadCM3 performed well for summer. The CSIRO Mk 2 overestimation can be explained in part by the problems in southwestern USA noted previously, so should be treated with caution. With the exception of CGCM2, however, all GCMs significantly overestimated the variability of winter precipitation.

Columns 6-9 of Table 1 show the changes in means projected by each GCM over a 100-year period. In this case, the values reported in the table are the "deltas" calculated as the *differences* in 30-year seasonal mean temperatures between 1961-90 and 2061-2090 and *ratios* of 30-year seasonal mean precipitation (2061-2090 means divided by 1961-1990 means). These results confirm the general magnitude of the increases in temperature simulated under each of the A2 and B2 scenarios reported earlier. They also show that, without exception, all the GCMs project increases in precipitation year-round, typically in the range of 10-15%, with the smallest increases occurring in summer.

The last section of Table 1 (i.e., columns 10-13), provides a comparison of the *change* in variability as projected by each GCM under each emissions scenario. In this case, the values reported are the ratios of the variances of seasonal means simulated by each GCM for the period 2061-2090 to those *simulated by the GCM* for 1961-1990. If the value is greater than 1.0 it indicates that simulated variability has increased, and conversely. These results are particularly interesting because they suggest that the A2 emissions scenario will produce significantly increased variability in seasonal temperatures (most ratios >1.0 for 2061-2090). The general trend under the B2 emissions scenario, however, is of reduced variability (most ratios <1.0 in the case of T_{min}, and several are less or very close to 1.0 for T_{max}). The CSIRO Mk 2 projections are the notable exception in that this GCM exhibited substantial increases in temperature variability for spring and summer under A2, to match the significant exaggeration of present-day variability for fall and winter already noted, with somewhat smaller increases under the B2.

The changes in variability of seasonal precipitation projected by the different GCMs were less clear. There appeared to be very little consistency either among the different models or between the two emissions scenarios. Again, discounting the CSIRO Mk 2 because of the problems outlined earlier, all the GCMs projected small to large increases in seasonal variability, although the magnitudes of these increases varied with season and GCM. The HadCM3 projected the greatest increases, year-round, although all models indicated greater interannual variability in spring precipitation.

Clearly, changes in temporal variability of climatic variables are not the entire story. Figures 3 and 4 provide a comparison of the long-term spatial changes in two climate variables as simulated by each GCM under each emissions scenario. The 30-year means of July minimum temperature and precipitation were

Table 1. Basic statistics for seasonal mean data from different GCM scenarios compared with historical temperature and precipitation data.

	Ratios of Variances (GCM / Observed)[a]				Changes in Means (2061-90) – (1961-90)[b]				Ratios of Variances (2061-90) / (1961-90)[c]			
Min. Temperature	Spring	Summer	Fall	Winter	Spring	Summer	Fall	Winter	Spring	Summer	Fall	Winter
CGCM2 - A2	0.81	1.29	0.57	0.98	5.32	4.20	3.86	6.87	2.23	1.74	1.19	1.41
HadCM3 - A2	1.02	0.68	0.50	0.82	4.14	4.15	4.95	5.32	1.37	4.06	2.97	1.65
CSIRO Mk2 - A2	1.11	0.97	3.89	2.33	7.20	5.51	6.37	8.41	3.63	3.97	1.21	1.31
ECHAM4 - A2	1.76	0.82	0.59	1.44	7.47	5.96	7.42	9.53	0.72	2.05	2.47	1.51
CGCM2 - B2	0.81	1.29	0.57	1.00	3.83	3.01	2.89	4.84	0.87	0.86	0.67	0.91
HadCM3 - B2	1.01	0.66	0.49	0.80	3.20	3.22	4.02	4.05	0.81	1.96	1.22	1.04
CSIRO Mk2 - B2	1.11	0.97	3.89	2.27	5.24	4.73	5.50	6.62	2.79	1.50	0.79	0.60
ECHAM4 - B2	1.76	0.82	0.59	1.44	4.99	3.94	5.32	7.09	0.82	1.01	1.24	0.97
Max. Temperature	Spring	Summer	Fall	Winter	Spring	Summer	Fall	Winter	Spring	Summer	Fall	Winter
CGCM2 - A2	0.47	0.85	0.50	0.69	4.63	4.28	4.01	5.63	2.89	2.47	1.44	1.19
HadCM3 - A2	0.89	0.73	0.42	0.63	3.87	4.55	4.77	4.76	1.37	3.21	3.67	1.55
CSIRO Mk2 - A2	0.51	1.09	0.84	0.29	5.46	4.34	4.23	5.20	4.10	3.12	1.92	2.11
ECHAM4 - A2	1.41	0.69	0.56	1.25	3.16	2.47	4.18	5.48	0.86	1.81	2.53	1.60
CGCM2 - B2	0.47	0.85	0.50	0.69	3.32	2.96	2.94	3.99	1.06	1.04	0.73	0.81
HadCM3 - B2	0.87	0.66	0.40	0.62	3.01	3.52	3.92	3.70	0.69	1.71	1.44	0.97
CSIRO Mk2 - B2	0.51	1.09	0.84	0.29	4.34	3.59	3.65	4.42	2.10	1.29	0.81	1.28
ECHAM4 - B2	1.41	0.69	0.56	1.21	4.01	3.67	4.73	6.37	0.89	1.01	1.05	0.81

	Ratios of Variances (GCM / Observed)[a]				Changes in Means (2061-90) / (1961-90)[b]				Ratios of Variances (2061-90) / (1961-90)[c]			
Precipitation	Spring	Summer	Fall	Winter	Spring	Summer	Fall	Winter	Spring	Summer	Fall	Winter
CGCM2 - A2	0.26	0.76	0.54	0.81	1.10	1.03	1.07	1.06	1.99	1.77	0.94	1.65
HadCM3 - A2	0.35	1.03	0.49	1.49	1.13	1.09	1.19	1.16	2.17	2.55	5.12	1.31
CSIRO Mk2 - A2	0.35	2.50	1.53	1.56	1.19	1.06	1.08	1.17	1.79	0.74	0.75	0.68
ECHAM4 - A2	0.41	0.73	0.75	1.31	1.11	1.09	1.14	1.19	2.36	1.72	1.24	2.74
CGCM2 - B2	0.26	0.76	0.54	0.83	1.09	1.05	1.07	1.06	1.16	2.34	1.67	1.93
HadCM3 - B2	0.32	0.91	0.50	1.57	1.11	1.09	1.14	1.14	1.32	2.13	3.46	1.08
CSIRO Mk2 - B2	0.35	2.50	1.53	1.56	1.15	1.09	1.07	1.11	1.86	2.31	0.63	0.70
ECHAM4 - B2	0.41	0.73	0.75	1.30	1.09	1.09	1.11	1.15	2.32	1.27	1.03	1.50

Notes: [a] These ratios compare variances of seasonal means for the period 1961-1990 obtained from historical observations, to those simulated for the same period by each GCM. Hence, a value of 1.0 would indicate near-perfect agreement in the spatially and temporally averaged variances.

[b] Changes in seasonal temperatures are reported as differences, whereas changes in seasonal precipitation are reported as ratios.

[c] These ratios compare variances of seasonal means simulated by each GCM for the period 2061-2090 to those simulated by the same GCM for 1961-1990. Hence, a value of 1.0 would indicate no simulated change in the spatially and temporally averaged variances over a 100-year period.

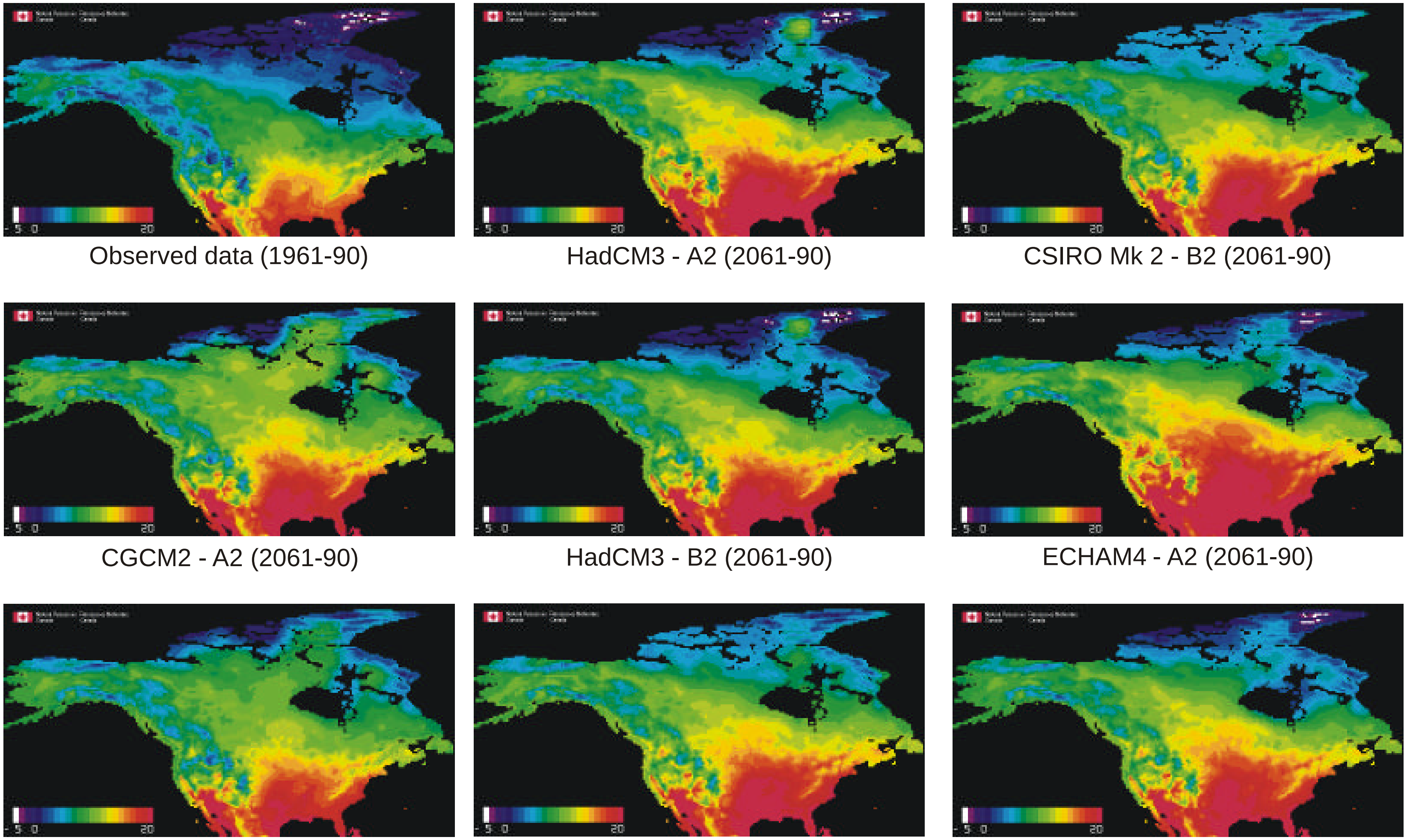

Observed data (1961-90) | HadCM3 - A2 (2061-90) | CSIRO Mk 2 - B2 (2061-90)

CGCM2 - A2 (2061-90) | HadCM3 - B2 (2061-90) | ECHAM4 - A2 (2061-90)

CGCM2 - B2 (2061-90) | CSIRO Mk 2 - A2 (2061-90) | ECHAM4 - B2 (2061-90)

Figure 3. Comparison of interpolated GCM scenario projections of July mean monthly minimum temperature (ºC) for the period 2061-2090. Also shown are interpolated climate station means for the period 1961-1990 (top left).

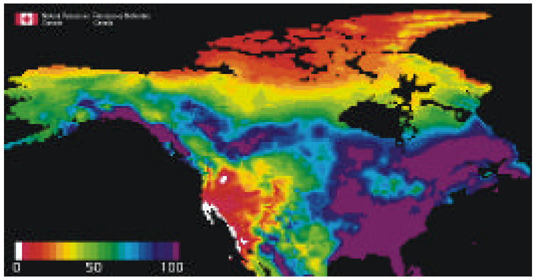

Observed data (1961-90)

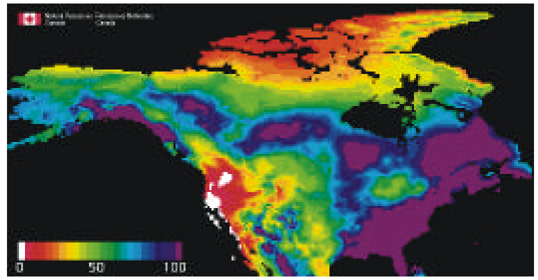

HadCM3 - A2 (2061-90)

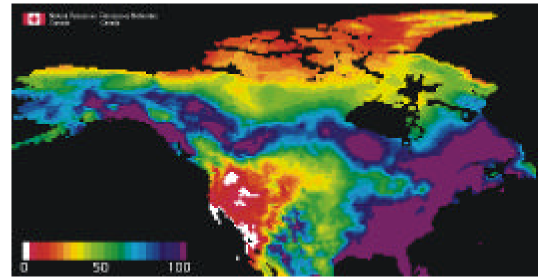

CSIRO Mk 2 - B2 (2061-90)

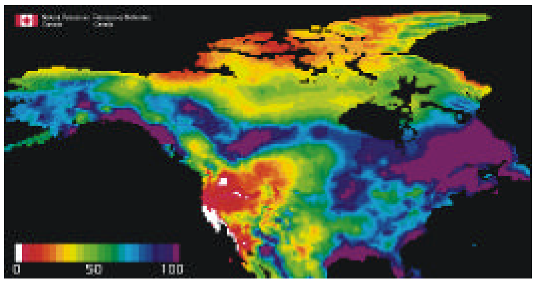

CGCM2 - A2 (2061-90)

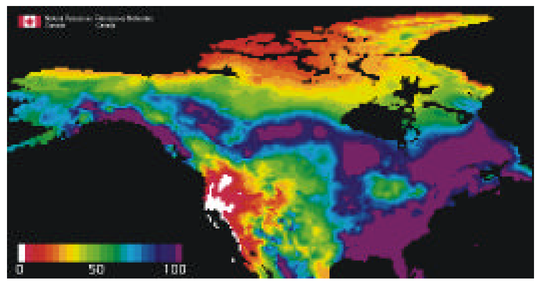

HadCM3 - B2 (2061-90)

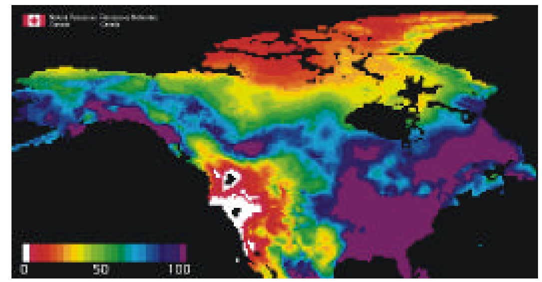

ECHAM4 - A2 (2061-90)

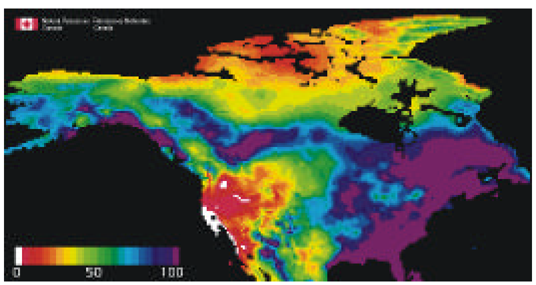

CGCM2 - B2 (2061-90)

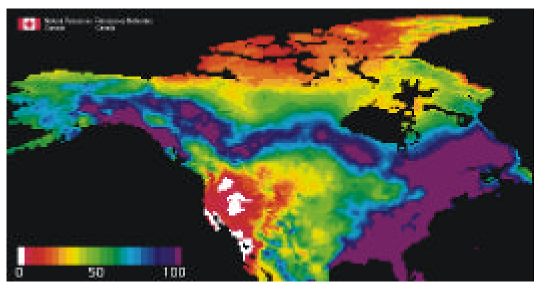

CSIRO Mk 2 - A2 (2061-90)

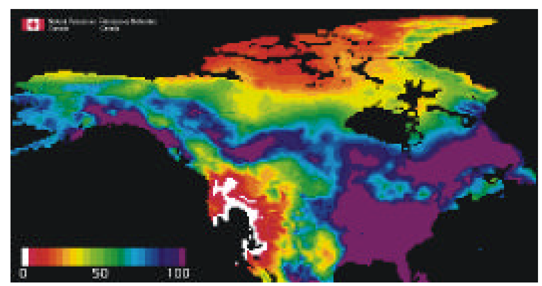

ECHAM4 - B2 (2061-90)

Figure 4. Comparison of interpolated GCM scenario projections of July mean monthly precipitation (mm) for the period 2061-2090. Also shown are interpolated climate station means for the period 1961-1990 (top left).

mapped at 0.5º latitude/longitude resolution both for 1961-1990 (observed data) and for each GCM projection of the 2061-2090 period. For each GCM, Figure 3 shows that spatialized projections of the general (continent-wide) increases in July minimum temperature are very similar under both emissions scenarios, differing only in that the A2 forcing invariably produces slightly higher mean temperatures than the B2. Only subtle differences among these projections result from inherent differences in the GCMs themselves. HadCM3 and ECHAM4 project conditions will be significantly cooler in the far north than do CGCM2 and CSIRO Mk 2. The ECHAM4 model forced by the A2 emissions scenario produces the most extensive region of increased temperature compared to 1961-90, but as we have already noted, the ECHAM4 A2 simulation exhibits an abrupt increase in $T_{\min}$ from the baseline, which seems unrealistic. If the ECHAM4 A2 result is discounted, the remaining maps are remarkably similar in all other respects.

Comparison of projected changes in mean July precipitation (Figure 4) shows rather greater differences between models and even between A2 and B2 forcings for some GCMs, but even here there are some striking similarities. In fact the general trend projected by the other models appears to be a general reduction in precipitation in the southern USA combined with slight increases in the boreal regions of Canada extending into southern Alaska. The drying of the south-eastern USA is generally more severe under the A2 emissions scenario, but ranges from a large region of reduced rainfall with CGCM2 to a smaller but drier region centered south of the Great Lakes with the Hadley and CSIRO models, to relatively little change from the baseline with ECHAM4. All the models project significant reductions in July rainfall for the western US coast, with ECHAM4 projecting the driest conditions.

5 DISCUSSION & CONCLUSIONS

In previous work, McKenney et al. (2001) and Price et al. (2001) used elevation as an independent variable, to capture fine-scale spatial variations in climate from station data interpolated across Canada. The dependence on elevation was found particularly important for the temperature, precipitation and vapour pressure fields. Figures 3 and 4 demonstrate the importance of that elevation effect in simulating the spatial variability of future projections of climate. Given the very poor representation of topography in present-day GCMs (due to their coarse horizontal resolution), omitting the elevation component determined from the observed data (i.e., the 1961-1990 normals) would cause the interpolated scenarios to resemble the original GCM projections—with only broad-scale gradients emerging latitudinally and across the Rocky Mountains. Normalizing the GCM output eliminates model bias, and combining the normalized data with the interpolated climate observations then provides a much richer image of future climate.

Eight high resolution climate change data sets have been developed, that should be useful for many finer-scale impacts studies, though there are some important caveats: In particular, these data sets are *scenario projections* and assuredly not predictions. Their value is not in the forecasts they provide for specific grid cells or geographic locations. Instead, they provide a set of continuously varying data that can be combined with other spatial data sets to provide a rich multi-dimensional mixture of possible future environments. These simulated environments, which are ultimately driven by a coarse-scale GCM integration, thus provide a means of driving climate-sensitive models with simulation data from several widely accepted GCMs .

The comparison of interpolated data from different GCMs shown in Figures 1-2 and reported in Table 1 is valid in so far as all data sets were processed identically. However, the comparison of these GCM scenarios with the historical time series raises a concern about area-weighting the calculation of the spatial averages. Given that a geographic map projection is being used, on an area-weighted basis, northern grid cells are contributing more to the calculated average than the southerly grid cells. This presents a problem when evaluating the historical data because the distribution of climate stations is uneven, and in fact the lowest station density typically occurs at the highest latitudes of Canada and Alaska, while the highest station density (which presumably indicates the greatest accuracy in the interpolated map product) occurs in the contiguous USA. Hence, in future work we will calculate the spatial averages accounting for the areas of each grid cell. Future work also includes production of a Canadian coverage using 10 km resolution on Lambert Conformal Conic (LCC) projection. The LCC is not a true equal area projection, but it greatly reduces the latitudinal distortion that occurs with geographic projections, hence a spatial average calculated over a large region is more meaningful. A further advantage of such projections is that when used as input to large-scale model simulations, they greatly improve the efficiency because the same area can be simulated with a more uniform density of grid points.

The data sets reported here will be suitable for driving a range of process models, where the objective is to investigate impacts of different climate scenarios *per se*. As with the GCM data themselves, however, the results obtained from such “impacts” models should not be taken as predictions, but rather as sets of possible outcomes located within a probability distribution determined by a plausible set of values for many variables including climate. Guided by available data, we attempt to capture what is known about the unique combination of conditions in each grid cell, but accept that it can never be completely correct. Repeating the simulations with different climate scenarios and comparing results for many grid cells will allow the impacts modeler to draw conclusions about the relative sensitivities of each region, and possibly, the relative probabilities of different outcomes.

These data sets were compiled to support comparison of the possible impacts of climate change on North American forest ecosystems. The Vulnerability and Impacts of North American Forests to Climate: Ecosystem Responses and Adaptation project (VINCERA), will compare simulations by three dynamic vegetation models, each driven by a common set of these climate scenarios. In addition they are being used to illustrate possible changes in the geographic scope of the climatic range of individual species (see http://g4.glfc.cfs.nrcan.gc.ca/ph_main.pl) Access to data can be obtained on application to the senior authors (DTP and DWM).

6 ACKNOWLEDGEMENTS

This work was supported by the Canadian Climate Change Action Fund, with particular encouragement from Elaine Barrow of Environment Canada's Canadian Climate Impacts Scenarios Group. Marty Siltanen and Fred Woslyng of Canadian Forest Service (CFS) in Edmonton provided assistance in downloading and preprocessing the GCM scenario data and documenting these procedures. Kevin Lawrence of CFS in Sault Ste. Marie provided programming support.

7 REFERENCES

Bugmann, H.K. and members of Working Group 2. 2000. Climate scenarios for forest impact assessments. In: T. Carter, M. Hulme, W.A. Cramer and R. Doherty (eds.) *Climate Scenarios for Agricultural, Ecosystem and Biological Impacts*, ECLAT-2 Second Workshop Report, Climate Research Unit, University of East Anglia, Norwich, U.K., pp. 80–83.

Houser, P., Hutchinson, M.F., Viterbo, P., Douville, H., Running, S.W. 2004. Terrestrial data assimilation. In: Kabat, P. et al. (eds) Vegetation, Water, Humans and the Climate. IGBP Global Change Series,Springer, Berlin, pp 273-287.

Hutchinson, M.F. 1995. Interpolating mean rainfall using thin plate smoothing splines. *Int. J. GIS* **9**(4), 385–403.

Hutchinson, M.F. 1989. A new method for gridding elevation and stream line data with automatic removal of pits. *J. Hydrol*., **106**, 211-232.

Hutchinson M.F. 1998a. Interpolation of rainfall data with thin plate smoothing splines: I two dimensional smoothing of data with short range correlation. *J. Geog. Information and Decision Analysis* **2(2)**: 152-167. http://publish.uwo.ca/~jmalczew/gida_4.htm

Hutchinson M.F. 1998b. Interpolation of rainfall data with thin plate smoothing splines: II analysis of topographic dependence. *J Geog. Information and Decision Analysis* **2**(2), 168-185. http://publish.uwo.ca/~jmalczew/gida_4.htm

Hutchinson, M.F. 2000. ANUSPLIN Version 4.0. http://cres.anu.edu.au/outputs/anusplin.php

Hutchinson, M.F. and P.E. Gessler, 1994. Splines—more than just a smooth interpolator. *Geoderma* **62**, 45–67.

IPCC (Intergovernmental Panel on Climate Change). 2000. Emissions Scenarios: Summary for Policymakers. Special Report of IPCC Working Group III. 20 pp. http://www.grida.no/climate/ipcc/spmpdf/ sres-e.pdf

Kittel, T.G.F., Royle, J.A., Daly, C., Rosenbloom, N.A., Gibson, W.P., Fisher, H.H., Schimel, D.S., Berliner, L.M. and VEMAP2 Participants. 1997. A gridded historical (1895-1993) bioclimate dataset for the conterminous United States. In: Proc. 10th Conf. Applied Climatology, 20-24 October 1997, Reno, NV. *Amer. Met. Soc.*, Boston, pp. 219–222.

Laprise, R., Caya, D., Frigon, A., Paquin, D. 2003. Current and perturbed climate as simulated by the second-generation Canadian Regional Climate Model (CRCM-II) over northwestern North America. *Climate Dynamics*, **21**, 405-421.

Lenihan, J.M. Neilson, R.P. 1995. Canadian vegetation sensitivity to projected climatic change at three organizational levels. *Climatic Change* **30**, 27-56.

McKenney, D.W., Kesteven, J.L. Venier, L.A. 2001. Canada's Plant Hardiness zones revisited using modern climate interpolation techniques. *Can. J. Plant Sci.* **81**(1), 117-129.

McKenney, D.W., Hutchinson, M.F., Papadopol,' P., Price, D.T. 2004. Evaluation of alternative spatial models of vapour pressure in Canada. 26th Conf. Agricultural and Forest Meteorology, 23-28 August 2004, Vancouver, BC. *Amer. Met. Soc.* Paper 6.2

Nalder, I.A., Wein, R.W., 1998. Spatial interpolation of climatic Normals: test of a new method in the Canadian boreal forest. *Agric. For. Meteorol.* **9**, 211–225.

Neilson, R. 1998. Simulated changes in vegetation distribution under global warming. In: Watson, R., Zinyowera, M., Moss, R. (eds.). The regional impacts of climate change: An assessment of vulnerability. Special Report of IPCC Working Group 2, Cambridge University Press, Cambridge, UK, pp. 441-456

New, M., Lister, D., Hulme, M., Makin, I. 2002. A high-resolution data set of surface climate over global land areas. *Climate Research*, **21**(1), 1-25.

Price, D.T., McKenney, D.W., Caya, D., Flannigan M.D., Côté, H. 2001. Transient climate change scenarios for high resolution assessment of impacts on Canada's forest ecosystems. Final report to Climate Change Action Fund, June 2001. http://www.cics.uvic.ca/scenarios/index.cgi?Other_Data#transienthighres

Price, D.T., D.W. McKenney, I.A. Nalder, M.F. Hutchinson and J.L. Kestevan. 2000. A comparison of statistical and thin-plate spline methods for spatial interpolation of Canadian monthly mean climate data. *Agric. For. Meteorol.* **101**, 81–94.

Rizzo, B., Wiken, E. 1992. Assessing the sensitivity of Canada's ecosystems to climatic change. *Climatic Change* **21**, 37–55.

VEMAP Members. 1995. Vegetation/ecosystems modeling and analysis project: Comparing biogeography and biogeochemistry models in a continental-scale study of terrestrial ecosystem responses to climate change and CO_2 doubling, *Global Biogeochemical Cycles*, **9**(4), 407-437.

Wilby, R.L., Dawson, C.W., Barrow, E.M. 2002. SDSM - a decision support tool for the assessment of regional climate change impacts. *Environmental Modelling and Software,* **17**(2), 145-157.

Wilby, R.L., Hassan, H., Hanaki, K. 1998. Statistical downscaling of hydrometeorological variables using general circulation model output. *J. Hydrol.* **205**, 1-19.